ARTIFICIAL MUSCLES

Strain-programmable fiber-based artificial muscle

Mehmet Kanik[1,2]*, Sirma Orguc[3]*, Georgios Varnavides[1,2,4], Jinwoo Kim[2], Thomas Benavides[3], Dani Gonzalez[5], Timothy Akintilo[6], C. Cem Tasan[2], Anantha P. Chandrakasan[3], Yoel Fink[1,2], Polina Anikeeva[1,2]†

Artificial muscles may accelerate the development of robotics, haptics, and prosthetics. Although advances in polymer-based actuators have delivered unprecedented strengths, producing these devices at scale with tunable dimensions remains a challenge. We applied a high-throughput iterative fiber-drawing technique to create strain-programmable artificial muscles with dimensions spanning three orders of magnitude. These fiber-based actuators are thermally and optically controllable, can lift more than 650 times their own weight, and withstand strains of >1000%. Integration of conductive nanowire meshes within these fiber-based muscles offers piezoresistive strain feedback and demonstrates long-term resilience across >10[5] deformation cycles. The scalable dimensions of these fiber-based actuators and their strength and responsiveness may extend their impact from engineering fields to biomedical applications.

Linear actuators simultaneously offering high temporal responsiveness, power-to-mass ratio, and strain and capable of operating across micrometer-to-centimeter spatial scales are poised to advance the fields of robotics, prosthetic limbs, and transportation (1). Although actuators based on shape-memory alloys (2), stimuli-responsive polymers (3–9), and carbon composites (10–14) offer lightweight, compact, and cost-effective alternatives to traditional hydraulic, pneumatic, and servo designs, their temporal responsiveness remains limited (15, 16). Recent research in polymer and composite actuators has drawn inspiration from cucumber tendrils that rely on differential swelling within their compartments to achieve high power-to-mass ratios and strains (17–20). Producing such structures at scale with tunable dimensions, however, presents a challenge. Furthermore, low-latency linear actuation without secondary transduction and integration of feedback mechanisms within these fiber-based artificial muscles has not been demonstrated (21).

We reasoned that differential thermal expansion within polymer bimorph structures comprising an elastomer and a thermoplastic polymer (22–24) amplified by the tendril-like spring geometry (fig. S1) would allow for linear actuation at low thermal stimuli. To produce bimorph structures with arbitrary lengths and lateral dimensions ranging from micrometers to millimeters, we relied on a scalable fiber-drawing process (25). Thermal drawing enables lateral size reduction of preforms by factors of 10^1 to 10^5 through controlled application of heat and tension while simultaneously delivering meters to kilometers of fiber (23, 26, 27). Unlike other fiber fabrication techniques such as electro- and jet-spinning, thermal drawing is applicable to multiple materials with a diversity of noncylindrical geometries (27). To be compatible with thermal drawing, the layers of the bimorph must, however, be composed of materials with similar viscosities at the drawing temperature. Simultaneously, maximizing the differences in thermal expansion coefficients (α) is necessary to achieve robust actuation. Guided by these constraints, a high-density polyethylene (PE, melting temperature T_m = 120°C, α = 1.3 × 10^{-4} K^{-1}) and cyclic olefin copolymer elastomer (COCe, melting temperature T_m = 84°C, α = 2.6 × 10^{-5} K^{-1}) were chosen as the constituents of the bimorph fibers (table S1). Finite element analysis was then applied to select a cross-sectional geometry that would optimize the thermal responsiveness of the bimorphs (fig. S2 and table S2). The final design of the bimorph fibers comprised identical PE and COCe layers with rectangular cross sections (25).

These fibers were then drawn from preforms composed of COCe and high-density PE blocks (25 mm by 8 mm cross section, 200 mm long) joined within a poly(methyl methacrylate) (PMMA) cladding (35 mm by 26 mm outer cross-sectional dimensions) (Fig. 1A and fig. S3). Prior to drawing, the preforms were annealed under pressure of 50 bar and temperature of 125°C to promote adhesion between the PE and COCe layers. By setting the drawing temperature (290° to 310°C) and the relative feed (v_f = 1 mm/min) and draw (v_d = 2 to 3 m/min) speeds, the cross-sectional area of the fiber was tuned between 50 μm by 35 μm and 5 mm by 3.5 mm over a 500-m length

(Fig. 1B). To further reduce the lateral dimensions, the fibers produced by the first drawing step were stacked within another PMMA preform and drawn at similar conditions to produce COCe-PE bimorph elements with cross-sectional areas as low as 13 μm by 8 μm (Fig. 1A and fig. S4). The thermomechanical mismatch between COCe and PE set an upper limit of processing 20 first-step fibers for every second-step PMMA preform. Increasing the number of fibers resulted in contraction failure of the preform (fig. S5). After drawing, the PMMA cladding was mechanically stripped to release the bimorph structures (Fig. 1C). The tension (70 to 100 mN) experienced by the fibers during drawing led to the formation of a spring-like shape upon PMMA cladding removal (coil diameter ~30 to 40 mm, fig. S6).

To produce actuated springs via strain programing from the bimorph fibers, these structures were cold drawn at strains of 50 to 1300%, which induced plastic deformation in PE (Fig. 1D). Upon release, the elastomeric COCe component attempted to contract to its original dimensions, and the resulting stress in the bimorph structure induced the formation of tendril-like springs (Fig. 1E and movies S1 and S2). The high prestrains between ~700 and 1300% were only tolerated by a subset of fibers, likely due to the manufacturing defects. The diameters of springs scaled with the cross-sectional dimensions of the precursor fibers, and a variety of springs could be obtained from the first and second iterative draws (Fig. 1, F and G) (25).

The fivefold mismatch in coefficients of the thermal expansion between the COCe and PE enabled rapid thermal actuation. Upon temperature increase, the PE underwent greater thermal expansion relative to COCe, which increased the tensile strain in COCe and induced further tightening of the springs (fig. S7) (25). Figure 1H demonstrates a 50% linear contraction in a fiber actuator with a 0.64 mm by 1 mm cross-sectional area in response to a temperature increase of ΔT = 14°C applied over 4 s.

We observed the spontaneous formation of unstable bifurcations, which are also found in cucumber tendrils and termed "perversions" by Darwin (28). The stochastic formation of these bifurcations is predicted by applying the Kirchhoff theory for thin rods to the fibers with elliptical cross sections (figs. S7 to S9) (19, 25). Although these structures do not substantially impede the thermal actuation performance, their formation could, at least in part, be circumvented by simultaneously releasing the ends of the fibers after the application of prestrain (25).

To optimize the thermal actuation performance, we investigated the effects of cold drawing parameters applied to COCe-PE bimorph fibers on the mechanical properties of the resulting fiber-based muscles. Whereas fibers composed of PE and COCe alone exhibited stress-strain characteristics of a tough plastic and an elastomer, respectively, the bimorph fibers exhibited intermediate behavior (Fig. 2A) (23, 29). Increasing the deformation rate from 10 to 50 mm/min

[1]Research Laboratory of Electronics, Massachusetts Institute of Technology (MIT), Cambridge, MA 02139, USA. [2]Department of Materials Science and Engineering, MIT, Cambridge, MA 02139, USA. [3]Department of Electrical Engineering and Computer Science, MIT, Cambridge, MA 02139, USA. [4]John A. Paulson School of Engineering and Applied Sciences, Harvard University, Cambridge, MA, USA. [5]Department of Mechanical Engineering, MIT, Cambridge, MA, USA. [6]Paul G. Allen School of Computer Science and Engineering, University of Washington, Seattle, WA 98195, USA.
*These authors contributed equally to this work.
†Corresponding author. Email: anikeeva@mit.edu

during the cold drawing of the bimorph fibers allowed for greater built-in strain within the resulting artificial muscles. Further increasing the deformation rate, however, reduced the amount of achievable strain (Fig. 2A). This was consistent with an increase in the yield strength and the elastic modulus in thermoplastic materials with increasing deformation rate (29, 30). For a given fiber, the spring diameter and the spring index of the actuators formed by cold drawing were controlled by the deformation rate and the maximum applied strain (Fig. 2, B to D). Consistent with the maximum allowable strain observed at 50 mm/min for fibers with 300 μm by 470 μm cross-sectional area, the spring diameters reached their minimum at this deformation rate (Fig. 2B). At a fixed deformation rate, increasing the strain applied to bimorph fibers during cold drawing produced actuators with smaller spring diameters and a greater number of turns per centimeter (Fig. 2C). Spring index (k) of the actuators increased with the spring diameter and the

actuation strain (Fig. 2D), resulting in higher work capacity (Fig. 2E). The latter was limited by the coil-to-coil contact at the highest actuation temperature. An increase in the prestrain decreased the spring diameter, and thus the spring index. Decreasing cross-sectional dimensions of the fibers yielded an increase in residual stress in the springs formed after the cold drawing process (Fig. 2F).

The force generated by the cold-drawn (maximum strain of 700%, 50 mm/min deformation rate) fiber-based muscles with cross-sectional areas of 300 μm by 470 μm was characterized by connecting the devices to a force gauge within a custom-designed characterization setup (Fig. 2G and fig. S10). A modulated broadband light supplied thermal stimuli, and a thermistor was placed near the fiber muscles to monitor the change in the temperature concurrent with the generated force measurements. Three-second illumination pulses separated by 10-s rest periods induced temperature gradients of $3.45 \pm 0.43°C/s$

($n = 6$ cycles), causing a force of 36.23 ± 5.42 mN in 5-cm-long fiber muscles (Fig. 2H). An actuation rate of 13.25 ± 1.66 N/s for a temperature increase rate of $1.11 \pm 0.12°C/s$ and a power-to-mass ratio of 75 W kg^{-1} surpassed the average power-to-mass ratio of human muscle (50 W kg^{-1}). Increasing the exposure times led to a proportionate increase in both heating and generated force (Fig. 2I). No decline in performance was observed across multiple actuation cycles at different temperatures (Fig. 2I). Artificial muscles produced from the miniature bimorph fibers with cross-sectional areas of 8 μm by 12.5 μm fabricated by the two-step thermal drawing were similarly evaluated for their actuator performance (Fig. 2, G and J, and figs. S11 and S12). A micro-Peltier was used to apply a thermal stimulus, and a thermistor was placed near the fiber muscles to monitor the change in the temperature concurrent with the generated force measurement (fig. S13). A temperature gradient of $11.09 \pm 0.55°C/s$ ($n = 10$ cycles) produced a
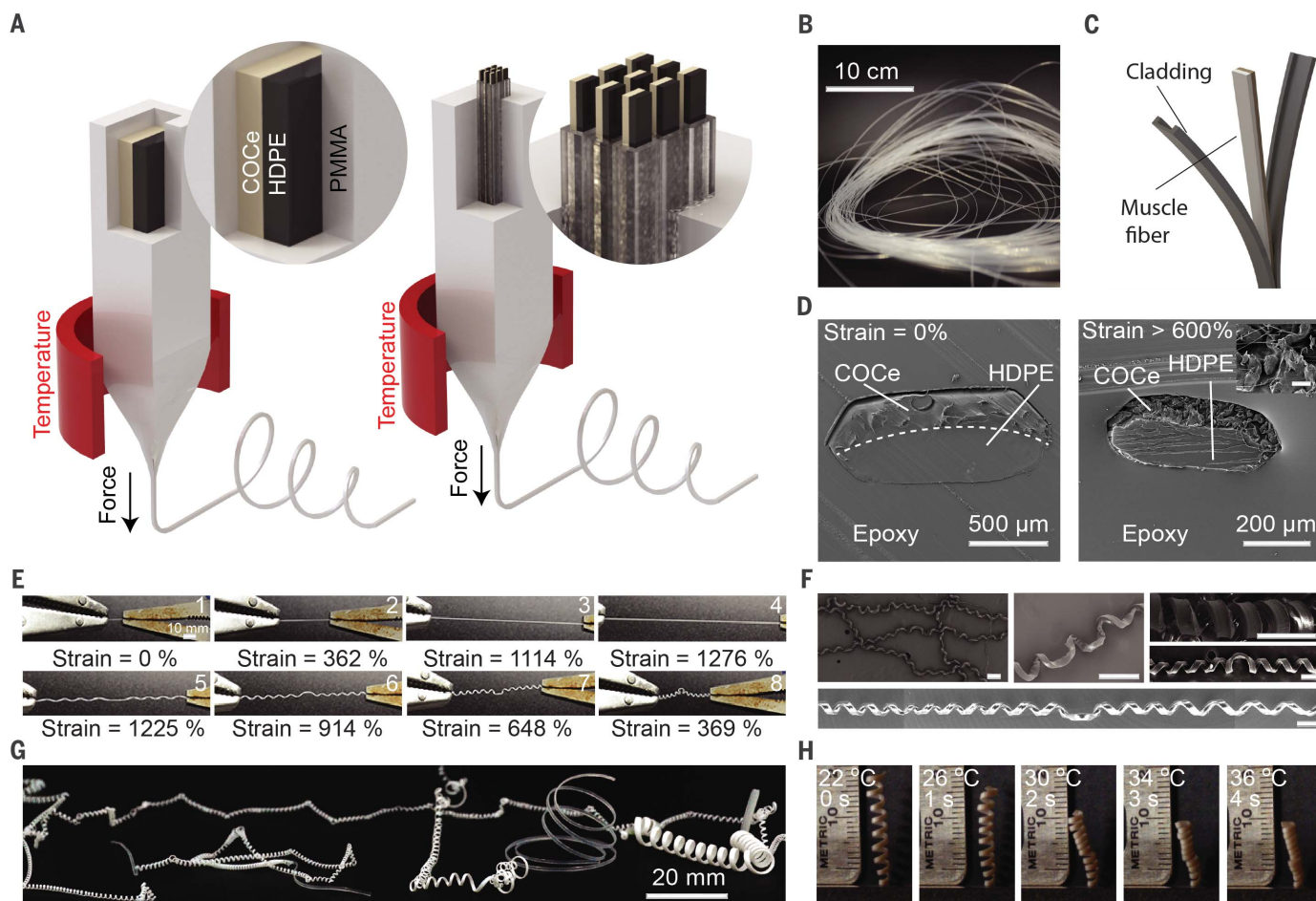
Fig. 1. Fabrication and morphological characterization. (**A**) Bimorph fibers produced via two-step thermal drawing. HDPE, high density PE. (**B**) Photograph of ~60 m of PMMA-encapsulated bimorph fibers. (**C**) Illustration of the PMMA cladding removal. (**D**) Cross-sectional scanning electron microscope (SEM) images of a fiber before and after cold drawing. Inset: COCe structure after stretching (scale bar: 20 μm).

(**E**) Cold drawing process for obtaining a spring actuator. Steps 1 to 4 show the stretching process. Upon release, shown in steps 5 to 8, the fibers formed springs. (**F** and **G**) Micrographs and photographs of the first-step and second-step artificial muscles [scale bars in (F): 200 μm]. (**H**) Fiber-based muscle contracting in response to a temperature increase of $\Delta T = 14°C$ (spring index: $k = 4.70$, 6 turns/cm).

force of 371 ± 40.7 μN in these 5-mm-long fiber muscles. The actuation rate of the miniature fiber muscle was 6.33 ± 0.72 N/s for a temperature increase rate of 130.3 ± 16.9°C/s, and the power-to-mass ratio was calculated as 90 W kg^{-1}. The power efficiency of the fiber-based muscles was found to increase with actuation strain and was higher for the fibers with larger cross-sectional areas (Fig. 2K). Actuator performance attributes of the fiber-based muscles are summarized in table S3. The devices (5 cm long, cross-sectional area 300 μm by 470 μm) were subjected to 300 cycles of thermal actuation over three consecutive days (ΔT = 13°C for 6 s,

followed by 30 s of rest, Fig. 2L), and no decline in performance was observed.

Fiber-based muscles were outfitted with conductive meshes of silver nanowires (AgNW, diameter = 70 nm and length = 50 μm) to enable monitoring of their contraction and elongation. These meshes were deposited directly onto the surfaces of the fiber muscles after the cold drawing process of the bimorph fibers, which was followed by the deposition of a protective stretchable layer of polydimethylsiloxane (PDMS) elastomer (23). Because percolation within the AgNW mesh changes with the contraction or elongation of the underlying substrates, AgNW-

coated fiber muscles act as piezoresistive sensors of deformation in response to stimuli. To evaluate this sensing ability, one end of the fiber muscles was connected to a direct current (DC) motor, and the resistance change was recorded by a voltage divider (Fig. 3A). A fractional resistance change of 0.47% was repeatable across ~12,000 cycles of 20% elongation (Fig. 3, B to D). Although a slow increase in baseline resistance was observed (Fig. 3, B and C), the relative change between extension and release cycles remained stable (Fig. 3D).

A single 5-cm-long fiber muscle with a cross-sectional area of 300 μm by 470 μm was able to
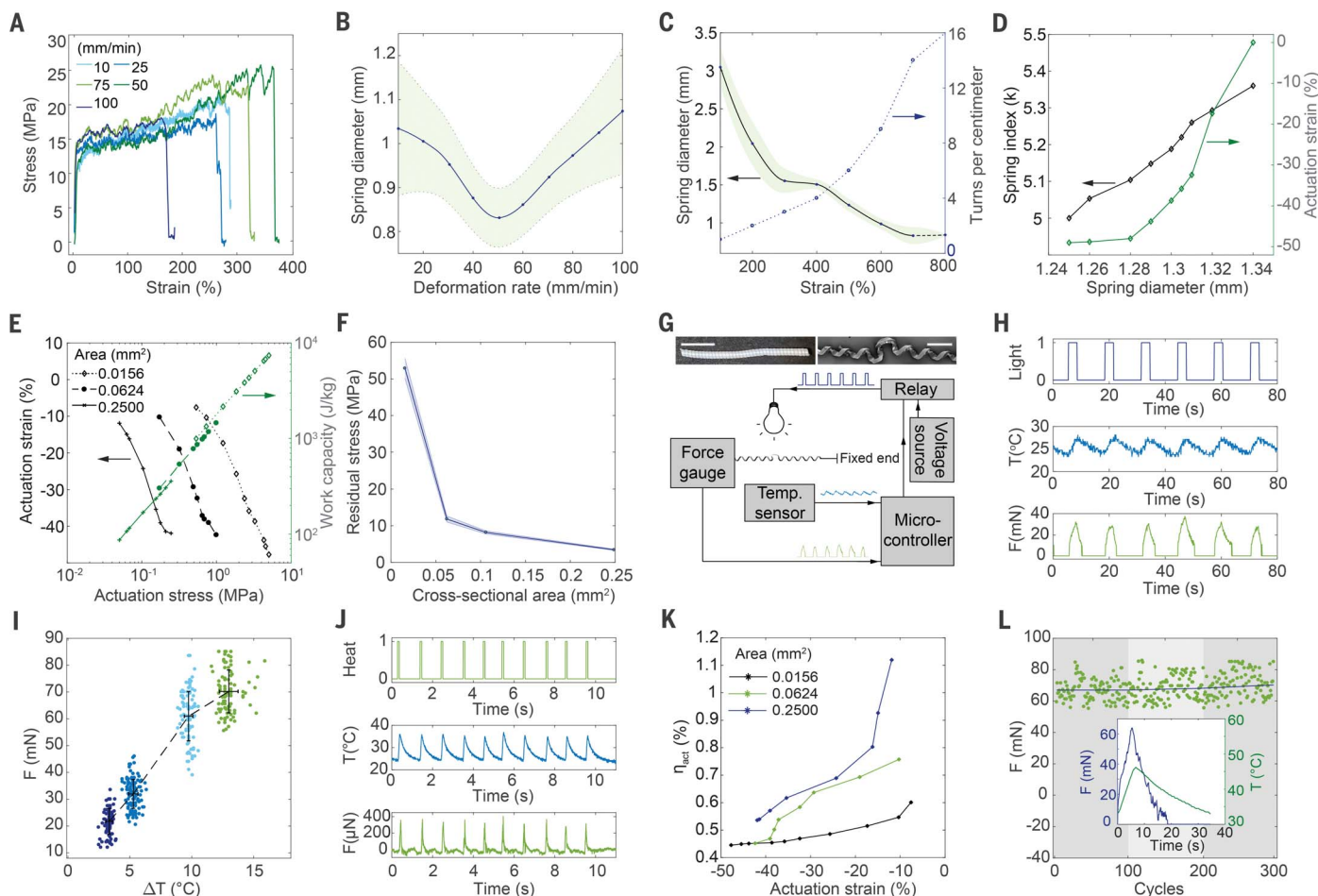

**Fig. 2. Mechanical characterization of fiber-based artificial muscle.**
(**A**) Stress-strain curves recorded at different extension rates for precursor fibers (without PMMA cladding) with a cross-sectional area of 300 μm 470 μm. (**B**) Change in the spring diameter with respect to the deformation rate. (**C**) Spring diameter and number of coils versus applied prestrain. Error bars and shaded areas represent average and standard deviation, respectively. The number of samples n = 5. (**D**) Change in the spring index with respect to spring diameter and actuation strain. (**E**) Change in the actuation stress-strain (gray) and work capacity (green). Attributes of the fibers are k = 6, 6 turns/cm (continuous line); k = 5, 10 turns/cm (dashed line); k = 5.5, 12 turns/cm (dotted line). (**F**) Change in the residual stress with respect to the cross-sectional area. (**G**) The setup used for the force measurement of the fibers with 300 μm by 470 μm cross section (scale bar, 5 mm). For the fibers with an 8 μm by 12.5 μm cross section (scale bar, 200 μm), a similar setup was used. The

optical heat source was replaced with a micro-Peltier heater, and a force gauge had a higher resolution. (**H**) Temperature and force responses to photothermal pulses collected for a fiber with 300 μm by 470 μm cross section (k = 5, 8 turns/cm). (**I**) Generated force versus the temperature difference (number of cycles 300) for fibers with 200 μm by 312 μm cross section (k = 5, 10 turns/m). Navy blue, dark blue, cyan, and green data point clusters represent different temperature ranges of 3.32 ± 0.26°C, 5.28 ± 0.37°C, 9.74 ± 0.34°C, and 12.98 ± 0.74°C, respectively. (**J**) Temperature and force responses to thermal pulses for a fiber with an 8 μm by 12.5 μm cross section (k = 4.6, 60 turns/cm). (**K**) Change in the efficiency with respect to actuation strain (blue line k = 6, 6 turns/cm; green line k = 5, 10 turns/cm; gray line k = 5.5, 12 turns/cm). (**L**) Force measured across 300 thermal actuation cycles applied over three consecutive days for a fiber with 200 μm by 312 μm cross section (k = 5, 10 turns/cm). Inset: A single actuation cycle.
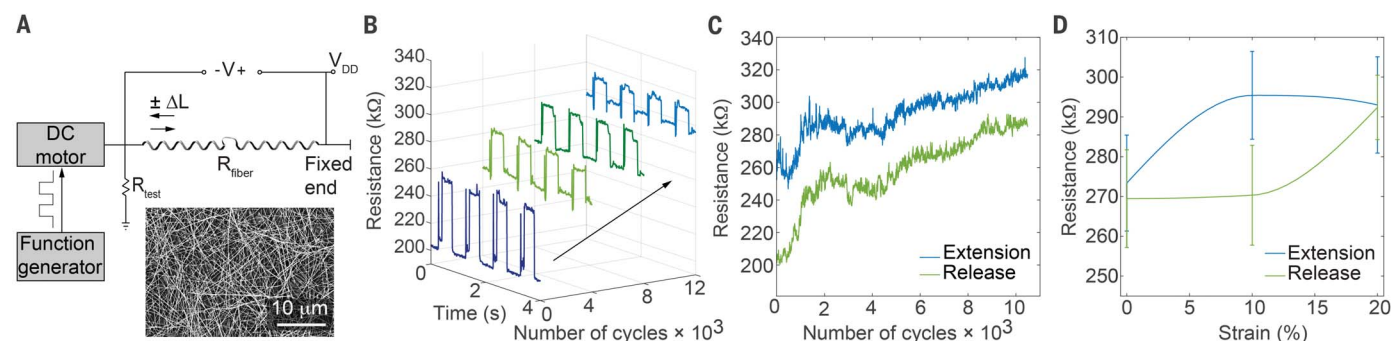
Fig. 3. Electrical feedback in fiber-based artificial muscle. (**A**) A schematic illustration of the setup for the resistance measurements for fibers with 300 µm by 470 µm cross-sectional area (k = 5, 8 turns/cm). Inset: A SEM image of silver nanowire mesh on the surface of a 300 µm by 470 µm^2 fiber-based muscle. (**B**) Resistance waveforms collected at different numbers of extension and release cycles. (**C**) The change in the extended and released resistance for ~12,000 cycles. (**D**) Hysteresis curve showing the resistance versus the applied strain for a single cycle of deformation. The lines represent the average and error bars represent the standard deviation.
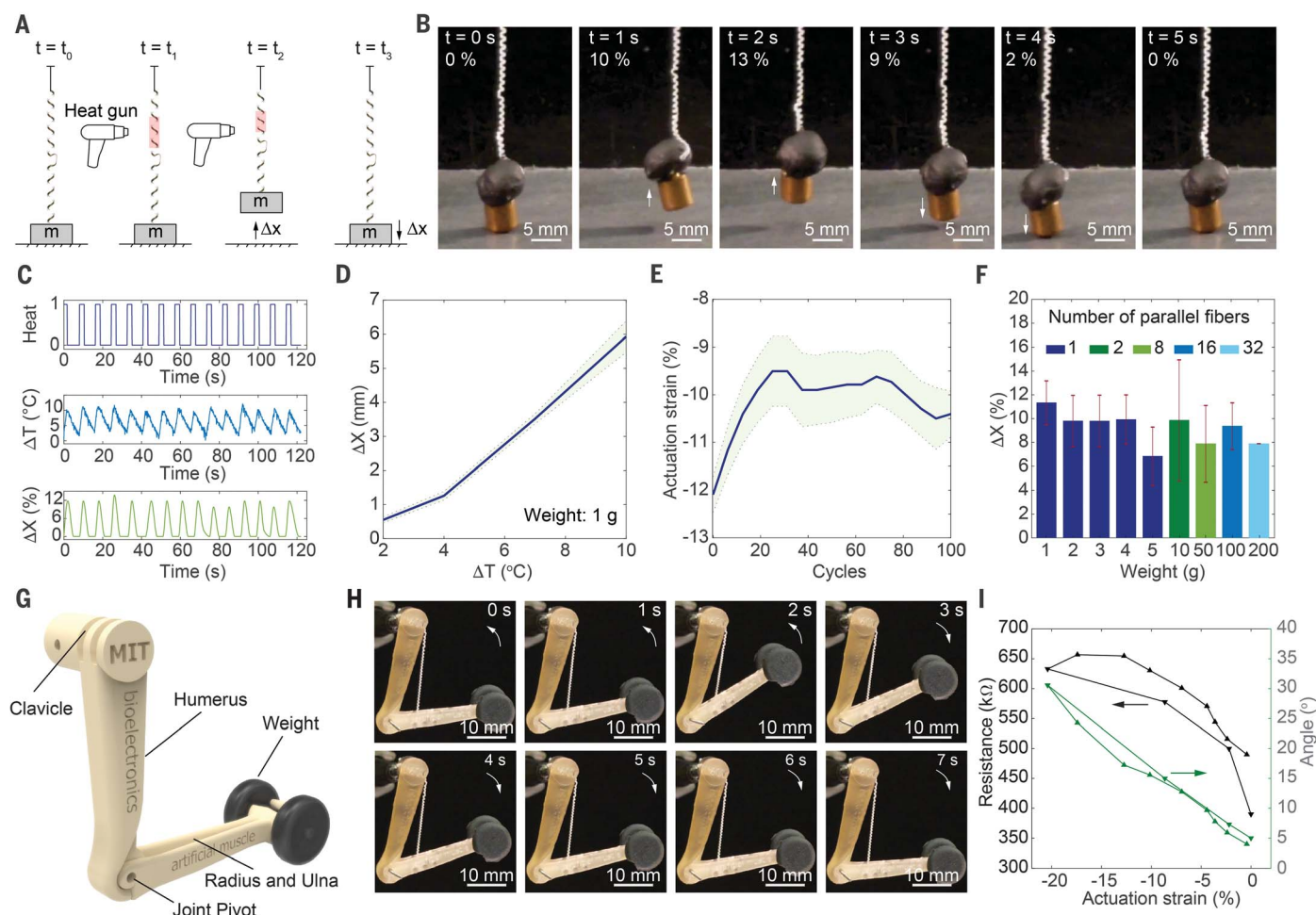
Fig. 4. Thermal actuation of fiber-based muscles. (**A**) Schematic illustration of the vertical lift experiment, where t is time, m is mass, and Δx is displacement. (**B**) A photographic time series collected during a displacement experiment in (A). The heat was applied in 2-s pulses separated by 6-s rest epochs. The load mass is 1 g. (**C**) Waveforms for the heat pulses (top), the corresponding change in the temperature at the fiber surface (middle), and the displacement of the 1-g load (bottom). (**D**) The vertical displacement Δx of a 1-g load in response to temperature increase ΔT. (**E**) Strain measurement across 100 cycles of thermal actuation. Solid and

dashed lines represent average and average ± 1 SD, respectively. (**F**) The maximum displacement for fiber bundles loaded with weights 1, 2, 3, 4, 5, 10, 50, 100, and 200 g. Error bars represent ± 1 SD. (**G**) A printed model of a weight-lifting artificial limb, inspired by a human arm. (**H**) A photographic time series of the artificial limb lifting a 1-g load. The heat was applied with a heat gun for 2 s and then followed by 5-s rest epochs. [(A) to (G)] Fiber cross-sectional area is 300 µm by 470 µm, spring index k = 5, and the number of turns per cm is 8. (**I**) The change in the fiber length, a piezoresistive strain feedback signal, and the angle of the arm for the experiment in (H).

lift a 1-g weight by 5.12 ± 0.76 mm (12% strain) in response to a thermal stimulus of ΔT = 10°C (from room temperature) delivered by a heat gun (Fig. 4, A and B, and movie S3). This behavior was reversible and repeatable across multiple cycles of 2-s heat pulses separated by 6-s rest periods, during which the fiber muscle cooled down to room temperature (Fig. 4C). The vertical displacement was linearly correlated with the thermal gradient (Fig. 4D). Permanent deformation was observed for temperature gradients $\Delta T \geq 50$°C, consistent with the thermomechanical properties of PE and COCe. Repeated application of 100 cycles of thermal actuation (ΔT = 8.8 ± 0.6°C) delivered reproducible actuation strains (10.1 ± 1.5%, Fig. 4E). Although an additive boost in strength was afforded by bundling multiple fibers in an oblique fashion, no observable change in stretchability was found (Fig. 4F, fig. S12, and movie S4).

To further illustrate the potential application of the fiber-based muscle as a model of biological muscle, we designed and printed a weight-lifting artificial limb inspired by a human arm (Fig. 4G). One end of the fiber muscle (300 μm by 470 μm cross section) was then affixed to the radius and ulna of the model forearm, while the other end was affixed to the clavicle. As found in the human arm, the joint between the humerus and the forearm was aligned with the clavicular muscle connection slot to maximize the displacement corresponding to a given bicep contraction (31). The artificial bicep was actuated by 2-s heat pulses (ΔT = 10°C) delivered by a heat gun, and relaxed upon cooling to room temperature (Fig. 4H and movie S5). The change in an angle between the forearm and humerus during operation correlated linearly with the fiber muscle contraction and extension (Fig. 4I). A miniature arm was used to lift a 1-g dumbbell, and the platform was scalable to a larger limb with greater weightlifting performance of 2 g afforded by two parallel fibers (movie S6).

This work presents a scalable strategy to produce fiber-based actuators with lateral dimensions ranging from millimeters to micrometers and arbitrary lengths. Cold drawing bimorph fibers composed of PE and COCe formed springs with the spring index and residual stress determined by the fiber cross-sectional dimensions, and the applied strain and deformation rate. The mismatch in the thermomechanical properties enabled reversible and repeatable thermal actuation. Conceptual demonstrations of load bearing and joint manipulation facilitated by the fiber-based artificial muscles indicate the possibility of their future applications in robotics and prosthetic limb technologies.

REFERENCES AND NOTES

1. M. Zupan, M. F. Ashby, N. A. Fleck, *Adv. Eng. Mater.* **4**, 933–940 (2002).
2. S. M. Mirvakili, I. W. Hunter, *ACS Appl. Mater. Interfaces* **9**, 16321–16326 (2017).
3. A. Maziz et al., *Sci. Adv.* **3**, e1600327 (2017).
4. A. Lendlein, R. Langer, *Science* **296**, 1673–1676 (2002).
5. J. Park et al., *Smart Mater. Struct.* **26**, 035048 (2017).
6. C. S. Haines et al., *Proc. Natl. Acad. Sci. U.S.A.* **113**, 11709–11716 (2016).
7. C. S. Haines et al., *Science* **343**, 868–872 (2014).
8. O. Kim, T. J. Shin, M. J. Park, *Nat. Commun.* **4**, 2208 (2013).
9. A. Lendlein, H. Jiang, O. Jünger, R. Langer, *Nature* **434**, 879–882 (2005).
10. K.-Y. Chun et al., *Nat. Commun.* **5**, 3322 (2014).
11. M. D. Lima et al., *Science* **338**, 928–932 (2012).
12. J. Deng et al., *Nat. Protoc.* **12**, 1349–1358 (2017).
13. S. H. Kim et al., *Sci. Rep.* **6**, 23016 (2016).
14. P. Chen et al., *Nat. Nanotechnol.* **10**, 1077–1083 (2015).
15. T. Mirfakhrai, J. D. W. Madden, R. H. Baughman, *Mater. Today* **10**, 30–38 (2007).
16. G.-Z. Yang et al., *Sci. Robot.* **3**, eaar7650 (2018).
17. M. H. Godinho, J. P. Canejo, G. Feio, E. M. Terentjev, *Soft Matter* **6**, 5965–5970 (2010).
18. M. H. Godinho, J. P. Canejo, L. F. V. Pinto, J. P. Borges, P. I. C. Teixeira, *Soft Matter* **5**, 2772–2776 (2009).
19. S. J. Gerbode, J. R. Puzey, A. G. McCormick, L. Mahadevan; L. M. Sharon J. Gerbode, *Science* **337**, 1087–1091 (2012).
20. Y. Cheng et al., *ACS Nano* **12**, 3898–3907 (2018).
21. K. Jung, K. J. Kim, H. R. Choi, *Sens. Actuators A Phys.* **143**, 343–351 (2008).
22. M. Shahinpoor, K. J. Kim, *Smart Mater. Struct.* **10**, 819–833 (2001).
23. C. Lu et al., *Sci. Adv.* **3**, e1600955 (2017).
24. M. Amjadi, M. Sitti, *ACS Nano* **10**, 10202–10210 (2016).
25. Materials, methods, and additional information are available as supplementary materials.
26. M. Yaman et al., *Nat. Mater.* **10**, 494–501 (2011).
27. S. Shabahang et al., *Nature* **534**, 529–533 (2016).
28. C. Darwin, *On the Movements and Habits of Climbing Plants* (London, 1865).
29. D. Kuhn, Howard Medlin, in *ASM Handbook*, vol. 8, *Mechanical Testing and Evaluation* (2000), pp. 26–48.
30. Y. Isogai et al., *Polym. Eng. Sci.* **58**, E151–E157 (2018).
31. E. P. Wismaier, H. Raff, K. T. Strang, *Vander's Human Physiology: The Mechanisms of Body Function* (McGraw-Hill, 2013).

Science

Strain-programmable fiber-based artificial muscle

Mehmet Kanik, Sirma Orguc, Georgios Varnavides, Jinwoo Kim, Thomas Benavides, Dani Gonzalez, Timothy Akintilo, C. Cem Tasan, Anantha P. Chandrakasan, Yoel Fink and Polina Anikeeva

Getting the most out of muscles
Materials that convert electrical, chemical, or thermal energy into a shape change can be used to form artificial muscles. Such materials include bimetallic strips or host-guest materials or coiled fibers or yarns (see the Perspective by Tawfick and Tang). Kanik *et al.* developed a polymer bimorph structure from an elastomer and a semicrystalline polymer where the difference in thermal expansion enabled thermally actuated artificial muscles. Iterative cold stretching of clad fibers could be used to tailor the dimensions and mechanical response, making it simple to produce hundreds of meters of coiled fibers. Mu *et al.* describe carbon nanotube yarns in which the volume-changing material is placed as a sheath outside the twisted or coiled fiber. This configuration can double the work capacity of tensile muscles. Yuan *et al.* produced polymer fiber torsional actuators with the ability to store energy that could be recovered on heating. Twisting mechanical deformation was applied to the fibers above the glass transition temperature and then stored via rapid quenching.
Science, this issue p. 145, p. 150, p. 155; see also p. 125

ARTICLE TOOLS	http://science.sciencemag.org/content/365/6449/145
SUPPLEMENTARY MATERIALS	http://science.sciencemag.org/content/suppl/2019/07/10/365.6449.145.DC1
RELATED CONTENT	http://science.sciencemag.org/content/sci/365/6449/125.full http://science.sciencemag.org/content/sci/365/6449/150.full http://science.sciencemag.org/content/sci/365/6449/155.full
REFERENCES	This article cites 35 articles, 7 of which you can access for free http://science.sciencemag.org/content/365/6449/145#BIBL
PERMISSIONS	http://www.sciencemag.org/help/reprints-and-permissions

Use of this article is subject to the Terms of Service